

Higgs-Induced Gravitational Waves: the Interplay of Non-Minimal Couplings, Kination and Top Quark Mass

Giorgio Laverda,^a Javier Rubio^b

^a*Centro de Astrofísica e Gravitação - CENTRA, Departamento de Física, Instituto Superior Técnico - IST, Universidade de Lisboa - UL, Av. Rovisco Pais 1, 1049-001 Lisboa, Portugal*

^b*Departamento de Física Teórica and Instituto de Física de Partículas y del Cosmos (IPARCOS-UCM), Universidad Complutense de Madrid, 28040 Madrid, Spain*

E-mail: giorgio.laverda@tecnico.ulisboa.pt, javier.rubio@ucm.es

ABSTRACT: We explore a minimal scenario where the sole Standard-Model Higgs is responsible for reheating the Universe after inflation, produces a significant background of gravitational waves and maintains the full classical stability of the electroweak vacuum. As the Higgs self-coupling runs toward negative values at high energy scales, a non-minimal interaction with curvature during a stiff background expansion era drives the Higgs fluctuations closer to the instability scale. This curvature-induced tachyonic instability leads to an intense production of Higgs particles, accompanied by a stochastic gravitational-wave background. The characteristic features of such signal can be directly correlated to the inflationary scale, the non-minimal coupling parameter and the top quark Yukawa coupling. We distinguish between three possible scenarios: absolute stability with low top quark masses, potential vacuum instability, and absolute stability with new physics above the instability scale. Our findings suggest that the detection of a peaked background of gravitational waves together with its inflationary tail has the potential to unveil the features of the Higgs effective potential at very high energy scales while providing a minimal explanation for the reheating phase and the emergence of the Standard-Model plasma in the early Universe. Unlike other studies in the literature, the generation of gravitational waves in our scenario does not depend on the quantum instability of the Standard Model vacuum.

Contents

1	Introduction	1
2	Effective Higgs potential with non-minimal curvature coupling	4
3	Stochastic gravitational-wave background	7
4	Probing the top quark mass with gravitational waves	8
4.1	Absolutely stable electroweak vacuum	10
4.2	Unstable electroweak vacuum	12
4.3	Independent heating mechanism	12
5	Stability beyond the Standard Model	14
6	Conclusions	17
A	Summary of parametric formulas	19
B	Setting up classical lattice simulations	19

1 Introduction

In recent years, the steady advancement of particle-collider experiments at the Large Hadron Collider has explored the Higgs sector up to energies of 13.6×10^3 GeV. The several orders of magnitude separating this energy range from plausible inflationary scales up to 10^{16} GeV leave us wondering about new physical phenomena in the Higgs sector that might have taken place in the early Universe. What role does the Higgs play in the history of the early Universe? One possibility is that it dominates the energy budget at very high scales. This assumption identifies the Higgs field with the scalar degree of freedom responsible for inflation, giving rise to Higgs inflation [1–19] (for a review see [20]). In the present work, we will consider the opposite alternative, namely that of a *spectator* Higgs within the early Universe [21–27]. In other words, the Higgs remains an energetically-subdominant quantum field during and shortly after inflation with a negligible backreaction on the gravitational background. In general, the whole Standard Model (SM) sector coupled to the Higgs can be considered to be in its vacuum state, while the Universe is still far from achieving a thermalised state.

In this setting, a non-minimal gravitational interaction can introduce significant new-physics effects in the Higgs sector. Indeed, the study of quantum fields on curved spacetimes leads to the conclusion that tree-level operators describing non-minimal gravitational interaction terms are generated naturally when renormalising the field’s energy-momentum

tensor [28]. Setting their coupling constants to vanish is an ad-hoc statement that depends on the energy scale. With these considerations, the physics of the Higgs field in the early Universe is dictated by the effective Lagrangian density

$$\mathcal{L} = \left(\frac{M_P^2}{2} - \xi H^\dagger H \right) R - g^{\mu\nu} (D_\mu H)^\dagger (D_\nu H) - \lambda \left(H^\dagger H - \frac{v_{\text{EW}}^2}{2} \right)^2 + \mathcal{L}_{\text{SM}} + \mathcal{L}_{\text{BSM}}, \quad (1.1)$$

where the effective potential of the Higgs doublet H depend on the quartic self-coupling λ and the electroweak vacuum expectation value v_{EW} . The additional term \mathcal{L}_{SM} contains all the SM fields beside the Higgs-field kinetic and potential terms and \mathcal{L}_{BSM} includes potential inputs from physics Beyond the Standard-Model (BSM) at high energy scales. For a Friedmann–Lemaître–Robertson–Walker (FLRW) metric $g_{\mu\nu} = \text{diag}(-1, a^2(t)\delta_{ij})$, the gravitational contribution to the Higgs mass is specified by the Ricci (or curvature) scalar $R = 3(1 - 3w)\mathcal{H}^2$, with $\mathcal{H} = \dot{a}/a$ the Hubble function. Consequently, a variation of the background expansion rate¹ of the Universe impacts the Higgs effective mass, making it possible for new phases to appear in the effective potential. This is the case for a period of stiff expansion following inflation, since the curvature scalar induces a large positive contribution for $w = -1$ and a large negative contribution for $w > 1/3$. For the remainder of this work, we will consider the case of *kinetic domination* to follow inflation when the departure from slow-rolling leads to a kinetically-dominated Universe with $w = +1$. Such a sequence of expansion phases can be found in a plethora of models including asymmetric α -attractors [29–32], variable gravity settings [33–35], axion-like dynamics [36] and non-oscillatory quintessential inflation [37–39]. The sign change of the Higgs effective mass at the transition between the two epoch triggers a so-called Hubble-Induced Phase Transition (HIPT) [27, 39–45].

During inflation, the large gravitational mass suppresses the Higgs quantum fluctuations, both super-horizon and sub-horizon, while preventing the generation of large isocurvature fluctuations [23, 24, 27, 46]. At the onset of kination, the large negative gravitational mass term induces a spontaneous symmetry-breaking with Hubble-scale-dependent true vacua. The Higgs quantum modes experience an exponential tachyonic amplification that quickly builds up the occupation number of infrared (IR) modes, followed by a cascade effect that turbulently populates ultraviolet (UV) modes as well.² It is precisely these amplified fluctuations that provide us with a way to study the post-inflationary spectator Higgs as they lead to three main outcomes:

1. The Universe can be heated by the non-perturbative tachyonic particle production and the corresponding exponential increase in the Higgs energy density. Requiring the Universe to be radiation-dominated at temperatures higher than the Big-Bang-Nucleosynthesis (BBN) temperature [60, 61] sets constraints on the space of model parameters.

¹In the present work it will not be necessary to embed the Higgs sector in a specific inflationary model. The only requirement is the quick onset of a phase of kination after inflation. We therefore maintain an agnostic and general approach to the inflaton dynamics.

²It is worth noting that this dynamic is significantly different from the well-known scenario of a resonantly-excited Higgs field interacting with an oscillating background [24, 25, 46–59].

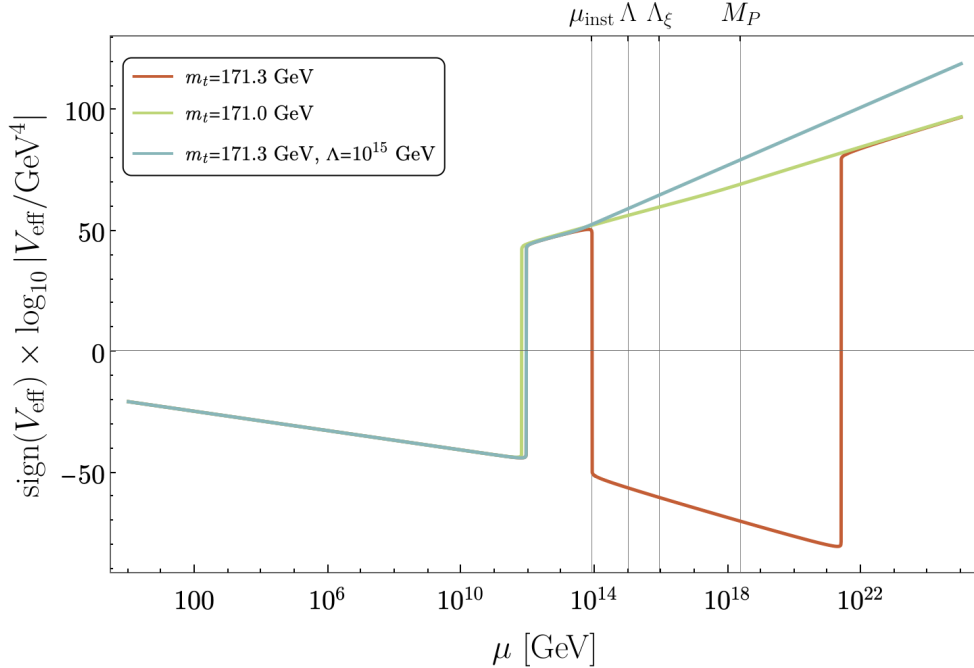


Figure 1. Higgs effective potential with a non-minimal gravitational coupling at the onset of kination for three prototypical scenarios: absolute stability (green line, $m_t = 171.0$ GeV), instability (red line, $m_t = 171.3$ GeV), stability with new physics as sextic operators at a typical scale $\Lambda = 10^{15}$ GeV (blue line, $m_t = 171.0$ GeV). The cut-off of the effective gravitational theory is given by $\Lambda_\xi = 9.2 \times 10^{15}$ GeV. The cosmological parameters have been set to $\nu = 20$ and $\mathcal{H}_{\text{kin}} = 10^9$ GeV.

2. Fluctuations that are significantly amplified can potentially probe the dangerous region above the instability scale μ_{inst} [62, 63], defined by the Higgs self-coupling running to negative values, i.e. $\lambda(\mu_{\text{inst}}) = 0$. Requiring the classical stability of our Universe imposes constraints on the top quark mass, as this is the major actor in the negative running of λ [10, 64].³
3. The generation of large spatial gradients leads inevitably to the production of a Stochastic Gravitational-Wave Background (SGWB). The signal is generated as the classicalised Higgs fluctuations enter the post-tachyonic non-linear dynamics, when the self-scattering process fragments the homogeneous patches inside the Hubble volume [67].

The SGWB signal generated by HIPTs offers a unique window into the post-inflationary physics of the spectator Higgs field. In particular, the specific features of the Gravitational-Wave (GW) spectrum allow us to explore the running of the Higgs self-coupling at high

³The values of the top quark masses used in this work refer to the top quark *pole* mass, m_t^{pole} , which differs from the *Monte Carlo reconstructed* mass, m_t^{rec} , typically extracted using event generators like PYTHIA or HERWIG. The difference between these quantities is approximately 1–2 GeV. Recent measurements confirm that m_t^{pole} is consistently lower than m_t^{rec} , with $m_t^{\text{pole}} = 170.5 \pm 0.8$ GeV [65] and $m_t^{\text{rec}} = 171.77 \pm 0.37$ GeV [66].

scales, by indirectly measuring the top quark mass. Three possible scenarios can occur. For top quark masses below the critical value of 171.035 GeV that guarantees absolute stability, the GW signal can peak at $\Omega_{\text{GW},0} \sim 10^{-6}$ and its typical frequency $f_{\text{GW},0} \sim 10^{10}$ Hz is tightly linked to the top quark mass. For higher top quark masses, the constraint on the stability of the electroweak vacuum bounds the inflationary scale from above, thus limiting the amplitude of the signal to $\Omega_{\text{GW},0} \lesssim 10^{-9}$. Notably, this GW background does not rely on the Higgs field crossing the instability scale, as considered, for instance, in [68]. In the presence of new physics around the instability scale, a prototypical sextic operator in the Higgs potential can restore the absolute stability of the potential, see Figure 1. In this case, a high-scale phase transition is still compatible with stability even for high inflationary scales or values of the top quark mass above the critical one.

We are interested in exploring a large range of non-minimal coupling parameters ξ , inflationary scales \mathcal{H}_{inf} and top quark masses m_t to identify the different scenarios that can be investigated by GW detection experiments. Our semi-analytical approach makes use of parametric formulas derived in previous works that condense numerous fully-fledged 3+1 classical lattice simulations into a few simple expressions [40, 67]. We also perform three high-resolution benchmark simulations in the extended scenario involving non-renormalisable operators to check the implications for the GW signal.

The present work is laid out as follows. We define the setup of the model including the Higgs effective potential and the tachyonic dynamics in Section 2, followed by the general study of the GW spectrum in Section 3. This picture is applied to the SM-Higgs scenario in Section 4, focussing on the differences between the cases of absolute stability, instability, and independent heating sector. Finally, in Section 5 we explore the possibility of the effective potential being stabilised by new physics at high scales. Section 6 contains some final remarks and ideas for further development.

2 Effective Higgs potential with non-minimal curvature coupling

The transition from an inflationary epoch to a kination-dominated phase introduces a significant tachyonic mass in the Higgs effective potential, triggering a second-order phase transition at high energy scales. This tachyonic instability can drive the Higgs fluctuations towards the unstable region of the effective potential as they become exponentially amplified. At high energies, the zero-temperature effective potential is approximately given by

$$V_{\text{eff}}(h) = \frac{1}{2}\xi R h^2 + \frac{1}{4}\lambda(\mu)h^4, \quad (2.1)$$

where h is the Higgs degree of freedom in the unitary gauge $H = (0, h/\sqrt{2})^T$. Notice that the energy scale μ entering the Renormalisation-Group-Improved (RGI) running $\lambda(\mu)$ is set as a combination of the background cosmological scale and the amplitude of the Higgs field itself $\mu = \mathcal{H} + h$, as per the standard prescription on curved backgrounds [21, 69]. To facilitate the analytical and numerical treatments, we make use of the following parametrisation [10] of the three-loop $\overline{\text{MS}}$ running of the Higgs self-coupling in the vicinity

of the instability scale,

$$\lambda^{3\text{loop}}(\mu) = \lambda_0 + b \log^2 \left[\frac{\mu}{q \text{ M}_{\text{P}}} \right], \quad (2.2)$$

which has an explicit dependence on the Higgs and top quark masses via the parameters λ_0 , b and q , namely

$$\begin{aligned} \lambda_0 &= 0.003297 \left(\left(\frac{m_h}{\text{GeV}} - 126.13 \right) - 2 \left(\frac{m_t}{\text{GeV}} - 171.5 \right) \right), \\ q &= 0.3 \exp \left[0.5 \left(\frac{m_h}{\text{GeV}} - 126.13 \right) - 0.03 \left(\frac{m_t}{\text{GeV}} - 171.5 \right) \right], \\ b &= 0.00002292 - 1.12524 \times 10^{-6} \left(\left(\frac{m_h}{\text{GeV}} - 126.13 \right) - 1.75912 \left(\frac{m_t}{\text{GeV}} - 171.5 \right) \right). \end{aligned} \quad (2.3)$$

We will assume from now on a fixed value of the Higgs mass $m_h = 125.2$ GeV [70] and focus on the impact the top quark mass has on the running of λ . A graphical representation of the effective potential can be seen in Figure 1, where the green and red lines exemplify the possible formation of a barrier in the SM effective potential at the instability scale μ_{inst} for different choices of top quark pole mass.

Imposing a stability constraint means ensuring that the tachyonically amplified fluctuations do not exceed the instability scale. The parametric description computed in a previous work [40] provides a convenient way to estimate the Higgs energy density at the end of the first semi-oscillation. This can be compared to the height of the barrier in the effective potential, setting with it a stability constraint, namely

$$\rho_{\text{tac}}(\mathcal{H}_{\text{kin}}, \nu, \lambda(h_{\text{min}})) < V_{\text{eff}}^{3\text{loop}}(h_{\text{max}}), \quad (2.4)$$

where ρ_{tac} is the Higgs energy density at the end of the tachyonic phase (first semi-oscillation of the field) and h_{min} , h_{max} indicate the positions of the new Hubble-induced minimum and the barrier. The tachyonically-enhanced energy density was found to follow the parametric behaviour

$$\rho_{\text{tac}}(\mathcal{H}_{\text{kin}}, \nu, m_t) = 16 \mathcal{H}_{\text{kin}}^4 \exp(\beta_1(m_t) + \beta_2(m_t) \nu + \beta_3(m_t) \log \nu), \quad (2.5)$$

obtained from 3+1-dimensional classical numerical simulations performed with the code *CosmoLattice* [49, 71]. The coefficients β_1, β_2 and β_3 in this expression are given in terms of $\nu = \sqrt{3\xi/2}$ and $n = -\log_{10}(\lambda(\mu))$, but the running in (2.2) allows us to trade the dependence on λ for a dependence on m_t , thus making explicit the connection between cosmological and SM parameters. The quantity \mathcal{H}_{kin} is the scale corresponding to the beginning of the kination phase which, for an instantaneous transition like the one under consideration, ⁴ can be identified with the inflationary scale $\mathcal{H}_{\text{kin}} \approx \mathcal{H}_{\text{inf}}$. A detailed

⁴One might wonder if taking into account the non-instantaneous transition from inflation to kination can lead to a non-negligible contribution to the Higgs energy density. This is important whenever the tachyonic process is inefficient, i.e. when the non-minimal-coupling induced vacuum is displaced at small field values. In general, a scalar field with a time-varying effective mass between inflation and kination undergoes a process of non-adiabatic particle production. This can lead to some initial excitation that can contribute to the final energy-density after the Hubble-induced phase transition. One can estimate the energy-density

discussion of the stability/instability scenarios was carried out in [27], alongside the study of the reheating stage in the Higgs, gauge and fermionic sectors, concluding that only the former is relevant for the macroscopic dynamics of heating.⁵ Here we only emphasise that the same set of parametric formulas derived in [40] allows us to quantify the course of the heating stage. Indeed, the first consequence of the tachyonic instability is the enhancement of the Higgs energy density and the reheating of the primordial Universe. To describe this phase, we make use of the *radiation* timescale at which the equation-of-state parameter for the Higgs field becomes $w_h = 1/3$,

$$z_{\text{rad}}(\nu, m_t) = \gamma_1(m_t) + \gamma_2(m_t) \nu, \quad (2.6)$$

and of the Higgs energy density

$$\rho_{\text{rad}}(\mathcal{H}_{\text{kin}}, \nu, m_t) = 16\mathcal{H}_{\text{kin}}^4 \exp(\delta_1(m_t) + \delta_2(m_t) \nu + \delta_3(m_t) \log \nu), \quad (2.7)$$

evaluated at z_{rad} , where $z = a_{\text{kin}}\sqrt{6\xi}\mathcal{H}_{\text{kin}}\tau$ is a rescaled conformal-time variable. The full expressions, including the numerical coefficients, can be found in Appendix A. The duration of the heating phase is encoded in the *heating efficiency* of the Higgs sector [78],

$$\Theta_{\text{ht}}^h \equiv \frac{\rho_h(a_{\text{rad}})}{\rho_\phi(a_{\text{rad}})}, \quad (2.8)$$

which measures the intensity of the non-perturbative tachyonic particle production. We also associate a *radiation temperature* to the Higgs-heated Universe [35]

$$T_{\text{ht}} = \left(\frac{30 \rho_h^{\text{ht}}}{\pi^2 g_*^{\text{ht}}} \right)^{1/4}, \quad (2.9)$$

with $g_*^{\text{ht}} = 106.75$ the SM number of relativistic degrees of freedom at energies above $\mathcal{O}(100)$ GeV and $\rho_h^{\text{ht}} = \rho_\phi^{\text{ht}}$ the total energy density of the Higgs field at the end of the heating phase. The fitting formula for ρ_{rad} in (2.7) allow us to estimate the heating temperature in terms of the model parameters $(\mathcal{H}_{\text{kin}}, \nu, m_t)$. Note that our definition of radiation temperature is agnostic about the achievement of a thermalised Universe. However, the thermalisation timescale is typically similar to the duration of the reheating phase [39, 79] and we will assume the Universe to be thermalised at the end of the heating stage.

produced by such process following the reference [72] and find it to be proportional to $\mathcal{H}_{\text{kin}}^4 \sqrt{\xi/12}$. For Higgs-like values of $\lambda(\mu)$, one concludes that the tachyonic production is more effective by several orders of magnitude. Modelling the non-instantaneous onset of kination has been considered in [73] by including an inflaton field together with a specific potential that defines a model-dependent transition.

⁵Resonant production of gauge bosons occurs as the Higgs oscillates in its effective potential. While this process involves successive exponential amplification, its efficiency is limited compared to the rapid tachyonic production of the Higgs itself. Assuming the Higgs oscillates uniformly in a quartic potential, resonant amplification proceeds with a Floquet index of $\mu_k \rightarrow \mu_{\text{max}} = 0.2377$ for $q = g^2/\lambda \gg 1$, typical for SM couplings [74]. Even under optimal conditions, it takes at least 10 oscillations for the energy density of bosonic fields to match that of the Higgs. The additional decay of gauge bosons into fermions does not significantly impact the heating timeline or vacuum stability constraints. However, non-Abelian interactions may aid in the thermalisation of the SM plasma, accelerating the approach to equipartition through boson scatterings and annihilations [13, 75–77].

If the breaking scale is sufficiently high $\mathcal{H}_{\text{kin}} \gtrsim 10^{5.5}$ GeV [27], the Higgs heating efficiency is large enough to dominate the heating stage with the constraint $T_{\text{ht}} > 5$ MeV [60, 61] generally fulfilled. In other words, the Higgs alone possesses the required energy density to start a phase of radiation-domination before BBN and no other heating mechanism is required. The parametric formulas in [40] can be used directly to compute the heating efficiency

$$\Theta_{\text{ht}}^h(\mathcal{H}_{\text{kin}}, \nu, m_t) = \frac{\rho_{\text{rad}}(\mathcal{H}_{\text{kin}}, \nu, m_t)}{3\mathcal{H}_{\text{kin}}^2 M_P^2} \left(1 + \frac{z_{\text{rad}}}{\nu}\right)^3, \quad (2.10)$$

and the heating temperature

$$T_{\text{ht}} \simeq 2.7 \times 10^8 \text{ GeV} \left(\frac{a_{\text{rad}}}{a_{\text{kin}}}\right)^{-3/2} \left(\frac{\Theta_{\text{ht}}^h}{10^{-8}}\right)^{3/4} \left(\frac{\mathcal{H}_{\text{kin}}}{10^{11} \text{ GeV}}\right)^{1/2}. \quad (2.11)$$

The successful heating of the Universe depends mostly on the scale of kination and on the non-minimal coupling parameter ν , making the threshold scale $\mathcal{H}_{\text{kin}} \simeq 10^{5.5}$ GeV independent from the chosen value of m_t . Indeed, for energy scales far below the instability scale, the running of the self-coupling converges to $\lambda(\mu) \simeq 0.1$ for all top masses, and only a weak dependence on ν remains for small values of non-minimal interactions.

3 Stochastic gravitational-wave background

The second major consequence of the initial amplification of the Higgs quantum modes is the generation of large fluctuations on sub-horizon scales. These “bubbly” features in the field distribution lead to the appearance of large spatial gradients [40], thus sourcing a strong GW signal [80]. This production phase is constrained to the interval between backreaction and the radiation timescale z_{rad} , during which the non-minimal and self-interactions have comparable magnitudes. By the radiation time, the system has quenched into a state of fragmented, small fluctuations. Hence, the GW spectrum possesses a clear peaked shape, as is typical for transient sources. The features of such GW signal were studied in detail with 3+1 classical lattice simulations in a recent work [67]. The general shape of the spectrum is well described by a prototypical broken-power-law shape function [81, 82]

$$\bar{\Omega}_{\text{GW}}(\mathcal{H}_{\text{kin}}, \nu, m_t; f) = \frac{\bar{\Omega}_{\text{p}}(a+b)^c}{\left[a\left(\frac{f}{f_{\text{p}}}\right)^{b/c} + b\left(\frac{f}{f_{\text{p}}}\right)^{-a/c}\right]^c}, \quad (3.1)$$

where the momentum and amplitude at the peak are given in terms of parametric functions obtained from numerical lattice simulations,

$$\begin{aligned} \kappa_{\text{p}}(\nu, m_t) &= \alpha_1(m_t) + \alpha_2(m_t)\nu, \\ \bar{\Omega}_{\text{GW,p}}(\mathcal{H}_{\text{kin}}, \nu, m_t) &= \left(\frac{\mathcal{H}_{\text{kin}}}{10^{10} \text{ GeV}}\right)^2 \exp[\beta_1(m_t) + \beta_2(m_t) \log \nu], \end{aligned} \quad (3.2)$$

where momenta κ are normalised with respect to \mathcal{H}_{kin} . As noted in the previous section, the dependence on the running of the Higgs self-coupling has been recast into a dependence

on the top quark mass thanks to the analytic form of the running in (2.2). The IR slope of the spectrum follows the expected causal behaviour $a = 3.00$ [83, 84], while the UV slope depends on the dynamics of the turbulent cascade following the out-of-equilibrium tachyonic particle production with typical values of the parameters $b = 152.34 - 6.57\nu$ and $c = 105.85 - 4.79\nu$. Spectra-related quantities are evaluated at the radiation time, i.e. at the end of the violent GW production process. Moreover, we have used the following normalisation of the GW energy density

$$\bar{\Omega}_{\text{GW}}(z_{\text{rad}}) \equiv \frac{\rho_{\text{GW}}(z_{\text{rad}})}{\rho_h(z_{\text{rad}})}, \quad (3.3)$$

with the critical density identified with the total energy density in the Higgs sector. Present-time frequencies and energy-densities can be computed using the expressions [85]

$$f_{\text{GW},0}(\nu, m_t) \simeq 1.3 \times 10^9 \text{ Hz} \frac{\kappa}{2\pi} \left(\frac{\mathcal{H}_{\text{kin}} a_{\text{rad}}}{10^{10} \text{ GeV}} \right)^{1/2} \left(\frac{\Theta_{\text{ht}}^h}{10^{-8}} \right)^{-1/4},$$

$$\Omega_{\text{GW},0}(\mathcal{H}_{\text{kin}}, \nu, m_t) = 1.67 \times 10^{-5} h^{-2} \left(\frac{100}{g_*^{\text{ht}}} \right)^{1/3} \times \bar{\Omega}_{\text{GW}}, \quad (3.4)$$

which depend on the duration of kination via the heating efficiency Θ_{ht}^h . As discussed in [67], the typical frequency of the spectrum does not depend on the scale of kination because of the cancellation caused by the common dependence on \mathcal{H}_{kin} of all relevant quantities. The heating efficiency Θ_{ht}^h and the scale factor a_{rad} at the radiation time can be readily evaluated using the parametric formulas in the Appendix A.

4 Probing the top quark mass with gravitational waves

In the most minimal scenario, the tachyonic phase in the Higgs dynamics is enough to exponentially enhance the Higgs energy density and lead to the reheating of the Universe. The details of the symmetry breaking depend on the running of the Higgs self-coupling in the chosen RGI scheme. By focussing on the dependence on the SM parameters m_h and m_t in (2.2) we can directly observe the influence that the top quark mass has on the spectrum of GWs. The specific characteristics of the GW signal would enable us to place indirect constraints to the top quark mass from gravitational physics.

The existence of an instability scale for larger values of the top quark mass forces us to consider two distinct possibilities. The scale of kination has to be a few orders of magnitude smaller than the instability scale to guarantee classical stability via the constraint

$$\rho_{\text{tac}}(\lambda(h_{\text{min}}), \nu) < V_{\text{eff}}^{\text{3loop}}(h_{\text{max}}). \quad (4.1)$$

Consequently, if the top quark mass is large and allows for the negative running of the Higgs self-coupling, the GW amplitude is going to be weaker due to the intrinsically lower kination scale. On the other hand, if the top quark mass is small and the Higgs is absolutely

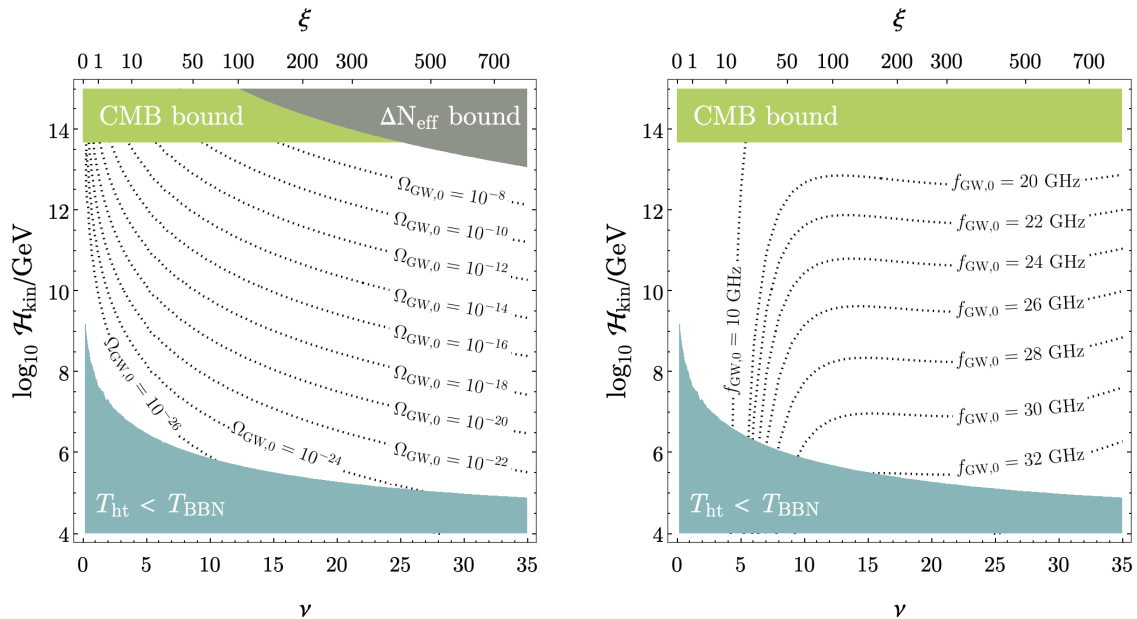


Figure 2. Energy density $\Omega_{\text{GW},0}$ and peak frequency $f_{\text{GW},0}$ of the GW spectrum at the present day as a function of \mathcal{H}_{kin} and ν . The top quark mass has been fixed to $m_t = 171$ GeV compatible with the absolute stability of the electroweak vacuum. The coloured regions indicate the areas excluded by the bound on the inflationary scale from CMB measurements (green), by the number of effective degrees of freedom at BBN (grey), and by the minimum reheating temperature (blue).

stable, the phase transition can happen at higher scales,⁶ up to the maximal bound on the inflationary scale $\mathcal{H}_{\text{max}} = 4.7 \times 10^{13}$ GeV [39] set by the Planck Collaboration [86], leading to a stronger GW signal.

The threshold separating these two scenarios is easily found from the running in (2.2). The solutions for $\lambda(\mu) = 0$ have a bifurcation point at $\lambda_0 = 0$ which implies a simple relation

$$\bar{m}_t = \frac{m_h + 216.87 \text{ GeV}}{2}, \quad (4.2)$$

giving us the largest top quark mass \bar{m}_t that is still compatible with the absolute stability of the SM vacuum. The best current measurement of the Higgs mass $m_h = 125.2 \pm 0.11$ GeV [70] corresponds to a critical top quark mass of $\bar{m}_t = 171.035$ GeV for its central value. In principle, below this threshold, the kination scale can be as high as \mathcal{H}_{max} but two observational constraints must be taken into account: reheating has to be achieved at temperatures above the BBN temperature and the contribution to total energy density by GWs cannot exceed the percentage allowed by the uncertainty on the number of effective

⁶The consistency of the spectator-field approximation requires the Higgs field non to backreact on the gravitational background and change the effective Planck mass, with the two conditions $\rho_{\text{tac}} \ll \rho_\phi$ and $\xi h_{\text{tac}}^2 < 0.1 \times M_P^2$ imposing an upper bound on the scale of kination. Due to the typical value of $\lambda(h_{\text{min}}) \approx 10^{-3}$, the parameter space we are considering is compatible with these bounds, see the discussion in [27, 40].

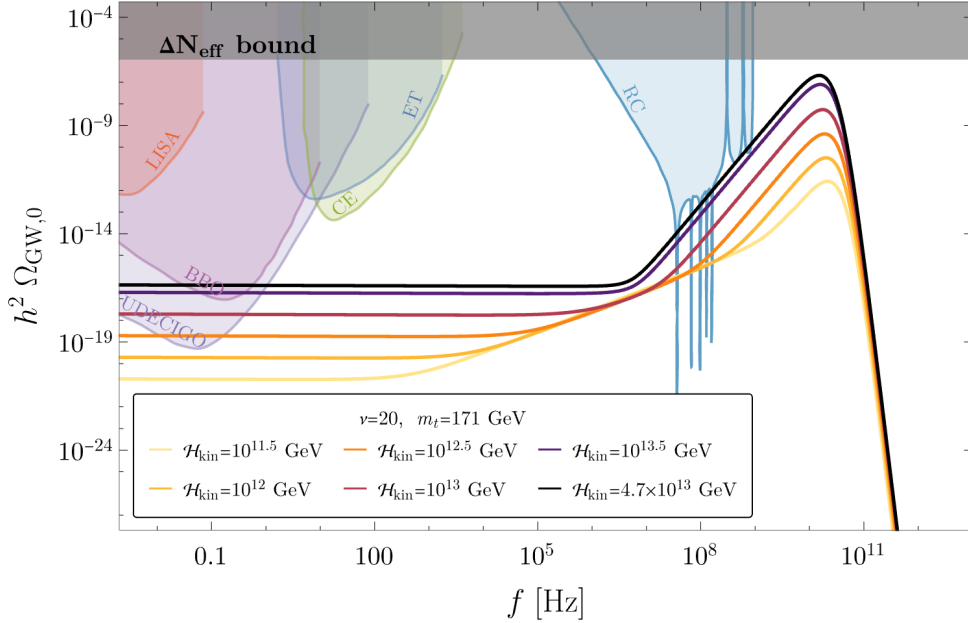


Figure 3. SGWB signal from a Higgs HIPT for different breaking scales compared to sensitivity curves of future GW detectors: Laser Interferometer Space Antenna (LISA) [87, 88], Big Bang Observer (BBO) [89, 90], UltimateDECIGO [91–93], Einstein Telescope (ET) [94, 95], Cosmic Explorer (CE) [96, 97] and Resonant Cavities (RC) [98]. The non-minimal coupling parameter is set to $\nu = 20$ while the top quark mass $m_t = 171$ GeV ensures the absolute stability of the Higgs vacuum.

relativistic degrees of freedom at BBN. The latter can be translated into the upper bound

$$h^2 \int \frac{df}{f} \Omega_{\text{GW},0} \lesssim 5.6 \times 10^{-6} \Delta N_{\text{eff}} = 1.1 \times 10^{-6}. \quad (4.3)$$

The effect these two constraints have on the parameter space can be seen in Figure 2. The bound on the maximal inflationary scale and on the effective number of relativistic degrees of freedom tends to exclude high breaking scales, while low-scale inflationary scenarios are also excluded from reheating arguments. These constraints are universal for any value of the top quark mass, since the Higgs self-coupling converges towards its IR value $\lambda \approx 0.1$ at low scales. Dotted lines indicate the energy density of the GW spectrum for different combinations of parameters \mathcal{H}_{kin} and ν , while the top quark mass $m_t = 171$ GeV guarantees the absolute stability of the Higgs vacuum. It is interesting to notice that for $10 \lesssim \nu \lesssim 30$ the peak frequency of the GW spectrum is almost independent of the non-minimal coupling to gravity and directly correlates a particular value of the top mass to a specific value of the kination scale \mathcal{H}_{kin} .

4.1 Absolutely stable electroweak vacuum

The full GW signal in the case of absolute stability $m_t < \bar{m}_t$ is displayed in Figure 3 for a subset of the parameter space with $\nu = 20$. Higher scales of kination produce stronger signals, as it is clear from the fitting formula for the GW amplitude (3.2) and its rescaling

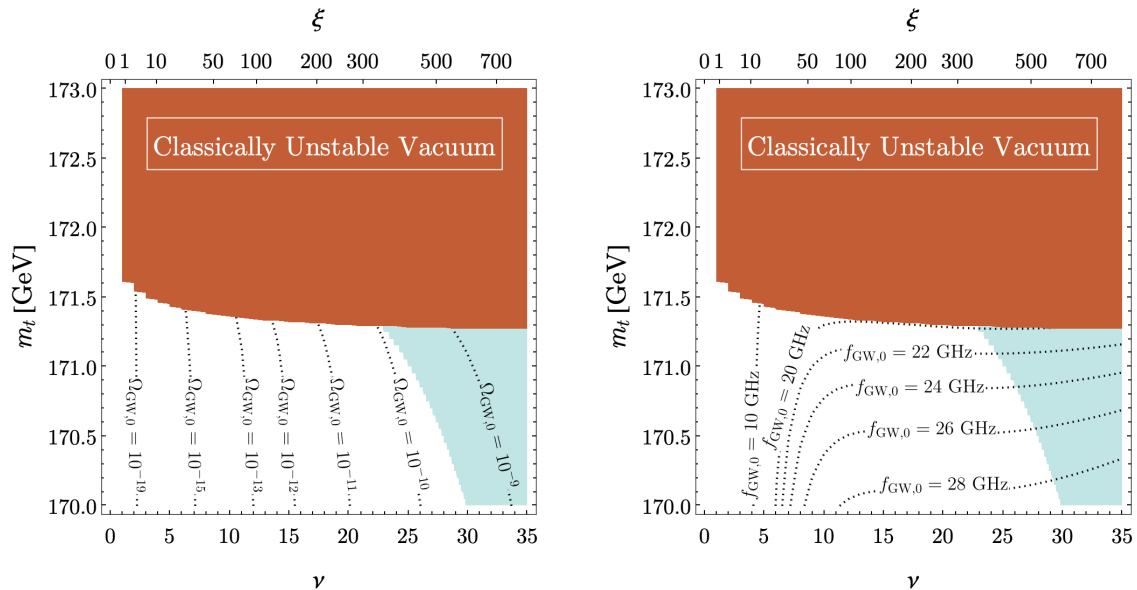


Figure 4. Energy density $\Omega_{\text{GW},0}$ and peak frequency $f_{\text{GW},0}$ of the GW spectrum at the present day for different values of the top quark mass and the non-minimal coupling parameter, with a fixed phase-transition scale $\mathcal{H}_{\text{kin}} = 10^{12}$ GeV. The light-blue-shaded area corresponds to a phase-transition signal within the sensitivity range of the Resonant Cavities experiment in [98].

(3.4). The typical frequency of the spectra from the phase transition is always within the range $10^{10} - 10^{11}$ Hz, restricting the possible detection of the peak to ultra-high frequency detectors [98–100]. On the other hand, the low-frequency part of the spectrum is dominated by the super-horizon inflationary tensor perturbations that are amplified as they reenter the horizon during the period of stiff expansion [101]. Their contribution to the spectrum is given by

$$\Omega_{\text{GW},0}^{\text{inf}}(f) \simeq 10^{-16} \left(\frac{\mathcal{H}_{\text{kin}}}{\mathcal{H}_{\text{max}}} \right)^2 \left(\frac{f}{f_{\text{pivot}}} \right)^{n_t}, \quad (4.4)$$

for modes reentering during radiation-domination, and by

$$\Omega_{\text{GW},0}^{\text{inf}}(f) \simeq 10^{-16} \left(\frac{\mathcal{H}_{\text{kin}}}{\mathcal{H}_{\text{max}}} \right)^2 \left(\frac{f}{f_{\text{pivot}}} \right)^{n_t} \left(\frac{f}{f_{\text{ht}}} \right), \quad (4.5)$$

for modes reentering during the stiff phase of kination, with $k_{\text{pivot}} = 0.002 \text{ Mpc}^{-1}$ the pivot scale at which \mathcal{H}_{max} is measured [86], f_{pivot} the frequency of the pivot scale, f_{ht} the frequency corresponding to the Hubble scale at the end of reheating and n_t the spectral tilt of inflationary perturbations. It is interesting to notice that the IR stochastic inflationary background is within reach of low-frequency detectors for sufficiently high kination scales. Consequently, two detection windows can simultaneously measure the kination scale in the low frequencies and the characteristics of the spectrum at higher frequencies. In this way, the full parameter space $(\mathcal{H}_{\text{kin}}, m_t, \nu)$ would be reduced to (m_t, ν) with a precise relation between m_t and ν . However, breaking this last degeneracy is a more complicated task that requires either the detection of the peak of the phase-transition signal or the detection of the

knees in the spectra indicating the size of the Hubble scale at reheating. Indeed, while the peak frequency is mostly dependent on the top mass, the non-minimal coupling parameter ν is the main actor in the duration of the heating stage, see [27]. The combination of a GW detection with constraints on the reheating temperature would, therefore, be able to characterise the Higgs effective potential at high scales.

4.2 Unstable electroweak vacuum

Considering now the case of $m_t > \bar{m}_t$, enforcing the stability condition in (2.4) sets an upper bound on the kination scale [27] and on the allowed top-mass range, see Figure 4. The instability region is determined by considering only the classical fluctuations of the Higgs field without taking into account the quantum tunnelling between vacua, which could further destabilise the low-scale vacuum. A quick estimate based on the Hawking-Moss and Coleman-de Luccia instanton solutions led to the conclusion that the electroweak vacuum lifetime is primarily affected by the classical overtaking of the barrier in the effective potential [27]. The task of computing a more realistic tunnelling rate in a time-dependent stochastic system with out-of-equilibrium fluctuations is an interesting but complicated problem by itself that goes beyond the scope of the present work [102–104].

As can be seen in Figure 4, the GW signal in the case of large top-quark masses is quenched by the small gravitational effective mass. For a fiducial value of $\mathcal{H}_{\text{kin}} = 10^{12}$ GeV the HIPT spectrum is typically below $\Omega_{\text{GW},0} \sim 10^{-9}$ and of comparable magnitude to the SGWB of amplified inflationary perturbations. Once more, it is possible to observe the tight relation between the top quark mass and the frequency of the GW signal, as noted also in Figure 2. This feature originates from the dependence of the peak frequency on the rescattering effects taking place in the non-linear phase. Larger values of $\lambda(\mu)$ lead to a quick cascade to smaller scales that produces a strong GW signal due to the large fluctuations. In this sense, a direct effect of the running of λ and the kination scale can leave an imprint on the GW signal.

Because of the stability bounds enforced on \mathcal{H}_{kin} , experiments at ultra-high frequencies would be able to primarily detect the blue-tilted inflationary spectrum, scaling proportionally to f instead of the typical f^3 -scaling of IR modes excited by causal sources [83, 84]. In Figure 4, the light-blue-shaded parameter space indicates that the phase-transition signal is visible by the resonant cavity experiment in [98]. The non-shaded area is allowed by stability constraints but it is characterised by a weaker signal generally obscured by the amplified inflationary perturbations. A precise evaluation of this situation requires a numerical analysis taking into account the horizon-reentering tensor perturbations during inflation, which act as a source term for the GW equation. This goes beyond the numerical simulations performed in [67], where a large separation of scales between the kination scale and the typical excited momenta is present. Such condition fails typically for very inefficient tachyonic production at low energy-scales or small non-minimal coupling parameters.

4.3 Independent heating mechanism

Although the tachyonic particle production in a HIPT scenario is a very efficient way to achieve a reheated Universe in non-oscillatory models of inflation, it is interesting to

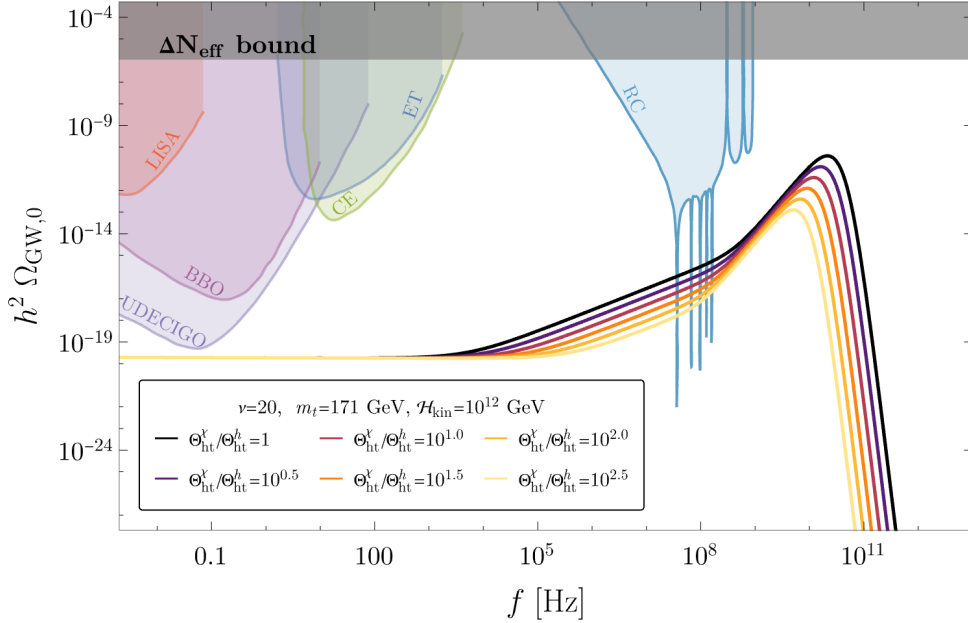


Figure 5. GW signal from the non-minimally coupled Higgs for different heating efficiencies of an independent sector Θ_{ht}^x compared to sensitivity curves of proposed GW detectors. The model parameters have been set to $\nu = 20$ and $m_t = 171$ GeV for a kination scale of $\mathcal{H}_{\text{kin}} = 10^{12}$ GeV.

consider the effects associated with an independent heating mechanism on the GW signal. This is particularly important for ensuring a successful reheating at low inflationary scales, $\mathcal{H}_{\text{kin}} \lesssim 10^{5.5}$ GeV, where the radiation temperature of the Higgs sector alone is generically below $T_{\text{BBN}} \simeq 5$ MeV. The details of the heating mechanism are not needed, as long as there exists a radiation-like sector whose energy density is greater than the Higgs'. In so doing, the heating stage is entirely described by the new sector's heating efficiency that we label with χ , namely $\Theta_{\text{ht}}^x \equiv \rho_\chi(a_{\text{rad}})/\rho_\phi(a_{\text{rad}})$. This quantity is the only additional free parameter we need to consider in our analysis. Since $\Theta_{\text{ht}}^x \geq \Theta_{\text{ht}}^h$ by construction, the heating temperature is higher than the Higgs-only scenario,

$$T_{\text{ht}}^x = \left(\frac{30 \rho_\chi^{\text{ht}}}{\pi^2 g_*^{\text{ht}}} \right)^{1/4} = \left(\frac{\Theta_{\text{ht}}^x}{\Theta_{\text{ht}}^h} \right)^{1/4} \times T_{\text{ht}}^h, \quad (4.6)$$

and kination is shorter-lived than in the standard case. The scaling of the GW signal from the moment of production to the present day is also affected, with a redshift in frequencies and a decrease in amplitude, as one can easily see in the formulas

$$f_{\text{GW},0}(\nu, m_t, \Theta_{\text{ht}}^x) \simeq 1.3 \times 10^9 \text{ Hz} \frac{\kappa}{2\pi} \left(\frac{\mathcal{H}_{\text{kin}} a_{\text{rad}}}{10^{10} \text{ GeV}} \right)^{1/2} \left(\frac{\Theta_{\text{ht}}^x}{10^{-8}} \right)^{-1/4},$$

$$\Omega_{\text{GW},0}(\mathcal{H}_{\text{kin}}, \nu, m_t, \Theta_{\text{ht}}^x) = 1.67 \times 10^{-5} h^{-2} \left(\frac{100}{g_*^{\text{ht}}} \right)^{1/3} \left(\frac{\Theta_{\text{ht}}^h}{\Theta_{\text{ht}}^x} \right) \times \bar{\Omega}_{\text{GW}}. \quad (4.7)$$

Notice that we recover the Higgs-only result if we assume the Higgs to be the only reheating sector $\Theta_{\text{ht}}^h = \Theta_{\text{ht}}^x$. In Figure 5, the combined effects of an independent heating sector are

visible in the relative positioning of the GW spectra. All model parameters have been fixed except from $\Theta_{\text{ht}}^{\chi}$, which can take on values much larger than Θ_{ht}^h . For highly efficient heating, the spectrum is peaked at lower frequencies but at the same time its amplitude is reduced, since the Higgs is energetically subdominant with respect to the external heating sector. The introduction of the χ -sector breaks the scaling relations that characterise the Higgs-only scenario by introducing a new independent energy scale. Since the duration of kination can be shortened, the amplification of the inflationary tensor perturbations is reduced and the phase-transition signal becomes more pronounced over the inflationary background the more efficient the heating sector is. The potential detection of a peaked GW signal at frequencies below the typical range in Figure 3 could be a smoking-gun clue for the existence of an external heating sector beyond the SM.

5 Stability beyond the Standard Model

The non-minimal coupling of the Higgs field to gravity makes the model under consideration intrinsically non-renormalisable, requiring it to be treated as an effective field theory valid up to a specific cut-off scale, $\Lambda_{\xi} = M_P/\xi$ [4, 7, 8, 77, 105–114], which may either signal the transition to a strongly coupled regime [113, 115–117] or the emergence of new degrees of freedom beyond the SM content [9] (for a review in the context of Higgs inflation see [20]). For the non-minimal couplings considered in this work, Λ_{ξ} is estimated to range from approximately 10^{16} to 10^{17} GeV, i.e. typically well above the SM vacuum instability scale. However, the validity of the low-energy effective field theory could be further reduced in the presence of additional sub-Planckian degrees of freedom beyond the SM content.

From a bottom-up perspective, such new physics would manifest itself as higher-dimensional operators suppressed by a cut-off scale $\Lambda \lesssim \Lambda_{\xi}$, determined by the thresholds and masses of the new particles as they are integrated out during the construction of the low-energy effective field theory. Interestingly enough, the inclusion of these non-renormalisable operators could potentially restore the convexity of the Higgs effective potential at high energies (see Figure 1), leading to the absolute stability of the electroweak vacuum irrespectively of the specific top-quark contribution. To investigate this possibility, we consider the impact of a prototypical non-renormalisable sextic operator, constructed from the gauge-invariant combination $H^{\dagger}H$ and the hypothetical cut-off scale of new physics Λ . The corresponding effective potential takes the form

$$V_{\text{eff}}(H) = (\xi R + m_h^2)H^{\dagger}H + \lambda(H^{\dagger}H)^2 + \frac{1}{\Lambda^2}(H^{\dagger}H)^3. \quad (5.1)$$

The inclusion of the sextic operator is expected to modify the β -functions of the theory [118], requiring their rederivation for a fully rigorous treatment of the problem. However, since the threshold effects associated with non-renormalisable operators become significant only in the vicinity of the characteristic scale, we will proceed by retaining the original three-loop running in (2.2) while incorporating the sextic operator as a simple tree-level term, thereby neglecting its energy dependence [119].

As illustrated in Figure 6, the presence of new physics at the scale Λ shifts the Planckian minimum of the effective potential to smaller scales, or even eliminates it entirely. This

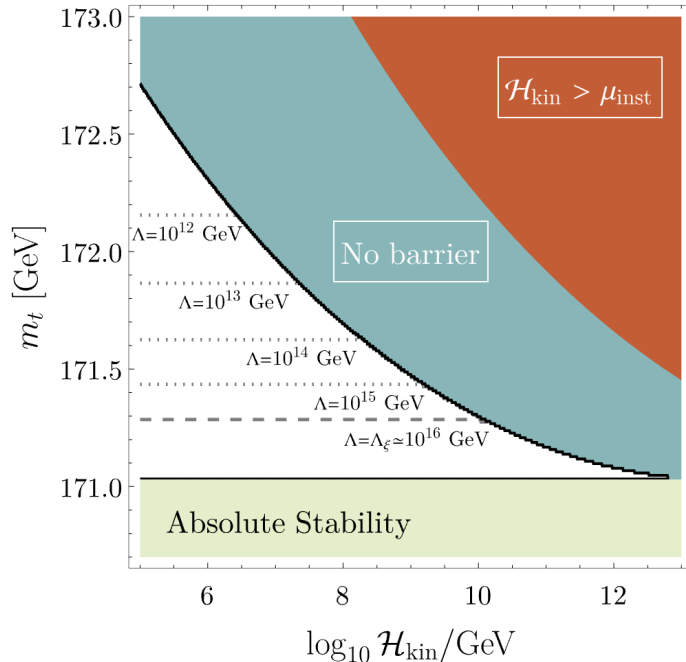


Figure 6. Impact of non-renormalisable sextic operators in the vacuum structure of the Higgs effective potential. The parameter space above the black line allows for the presence of only one minimum at high scales. The red area indicates that the instability scale is probed already during the inflationary stage, while the blue area indicates that the non-minimal curvature interaction suppresses the quartic barrier. The light-green area indicates absolute stability for $m_t \leq \bar{m}_t$, where only the low-scale minimum is present. The metastable scenario involving two minima is realised in the white area for the general case of the Standard-Model only effective potential. Including the sextic interaction term $(H^\dagger H)^3/\Lambda^2$ leads to a shift in the absolute stability bound, indicated by the dotted lines for different values of the cut-off scale Λ . The model parameters have been fixed to $m_h = 125.2$ GeV and $\nu = 20$, leading to an instability scale of $\mu_{\text{inst}} = 8.3 \times 10^{13}$ GeV and an effective-field-theory cut-off scale $\Lambda_\xi = 9.2 \times 10^{15}$ GeV (dashed line).

figure provides a direct representation of the different phases of the model at the time of symmetry breaking, i.e. at the onset of kinetic domination. In the absence of new physics, the classical dynamics of the Higgs fields must be generally checked for instability within the parameter space corresponding to the white area, while absolute stability is ensured only for top quark masses below the critical value of $\bar{m}_t = 171.035$ GeV. If the inflationary scale \mathcal{H}_{kin} is significantly higher than the instability scale μ_{inst} , the potential lacks a barrier and only the high-scale vacuum is present. The inclusion of sextic interactions stabilises the potential by restoring convexity at high scales. A large cut-off scale Λ is enough to ensure stability for low top quark masses, while a smaller Λ can stabilise the potential for a wider range of masses. As a result, the critical boundary at \bar{m}_t shifts upwards, as indicated by the dashed lines in the figure, thus expanding the parameter space associated with absolute stability. Notice that this analysis concerns only the overall vacuum structure of the potential at the time of symmetry breaking for a specific value of non-minimal

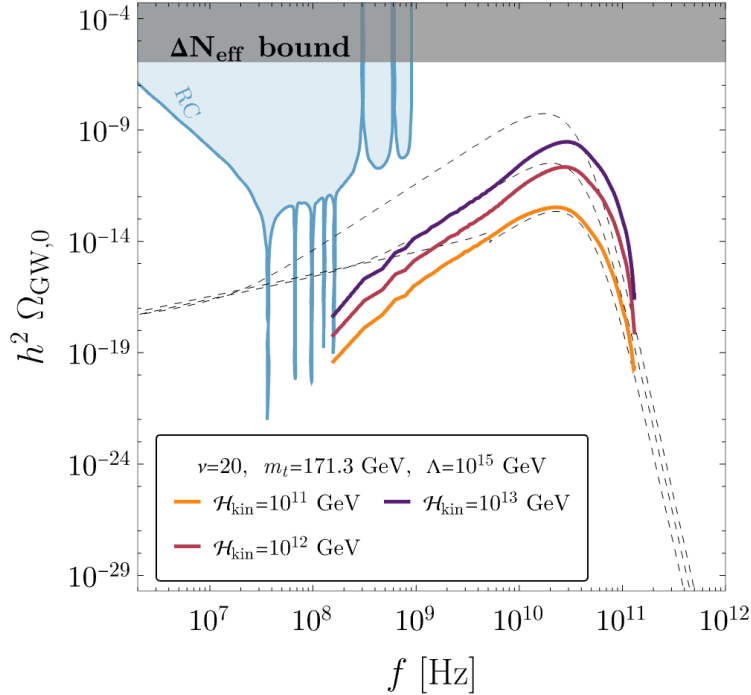


Figure 7. Present-day SGWB generated by the non-minimally coupled Higgs in the presence of higher order operators in the effective potential. Different colours correspond to different choices of kination scale \mathcal{H}_{kin} in our benchmark simulations, while the cut-off scale of new physics has been set to $\Lambda = 10^{15}$ GeV. The remaining model parameters have been set to $\nu = 20$ and $m_t = 171.3$ GeV. Dashed lines indicate the corresponding GW signals shown in Figure 3 for $m_t = 171$ GeV and $\mathcal{H}_{\text{kin}} = 10^{11}, 10^{12}, 10^{13}$ GeV.

coupling parameter and does not include the Higgs dynamics.⁷

Within the newly stabilised region, we turn once again to 3+1 classical lattice simulations. The main advantage of this numerical technique consists in the accurate description of the non-linear field dynamics and the prediction of the associated GW signal. The setup behind the implementation via the code *CosmoLattice* [71, 120] is described in Appendix B. For this discussion, it suffices to state that the numerical model incorporates the complete potential in (5.1), along with its parametric three-loop running (2.2). The simulations are initialised at the time of symmetry breaking, i.e. at the transition between inflation and kination, and evolved for at least two e-folds on a kination background to capture the GW spectrum after the end of the non-linear regime. This implementation follows the established methods already tested in previous studies, including the SM Higgs scenario without new physics [27] and the prototypical case of a scalar singlet at tree level [40, 67]. We consider three benchmark points for $\mathcal{H}_{\text{kin}} = 10^{11}, 10^{12}, 10^{13}$ GeV, while we keep the scale of new physics at $\Lambda = 10^{15}$ GeV. In order to assure the covering of all relevant

⁷In general, for the parameter space under consideration, the Hubble scale at the end of the first semi-oscillation of the field is about three orders of magnitude smaller than \mathcal{H}_{kin} . Qualitatively speaking, this difference shifts the black boundary in Figure 6 to higher values of \mathcal{H}_{kin} .

momenta, we perform simulations on a large grid of $N = 960$ lattice points per side.

The SGWB generated by the phase transition is presented in Figure 7. After extracting the spectrum at the timescale z_{rad} defined in (2.6), we rescale it to the present time using the formulas (3.4), assuming a typical value of $\lambda = 10^{-3}$ for renormalisation scales in the range $\mathcal{H}_{\text{kin}} = 10^{11} - 10^{13}$ GeV. For IR momenta, we recover the causal spectral slope proportional to f^3 , while the UV portion of the spectrum is noticeably changed. The reason lies in the more efficient turbulent cascade [79] towards UV modes induced by the sextic interaction. Consequently, the position of the peak is shifted to higher frequencies as compared to the absolutely-stable scenario (dashed lines in Figure 7) and its amplitude is reduced. Notice that this effect cannot be explained by the use of two different values of the top mass in the figure, since the peak frequency tends to decrease with higher top masses in the absolutely stable case, see Figure 6. The same turbulent process is responsible for the fast population of high-momentum modes, which flattens the overall tilt of the UV tail. These considerations are further supported by the gradual shift towards the UV of the BSM spectra with respect to the SM case as the scale of kination increases. Indeed, the SGWB matches well what one would expect from the absolute stability case for $\mathcal{H}_{\text{kin}} = 10^{11}$ GeV, since the classicalised Higgs fluctuations are well within the instability scale. However, at higher kination scales, the sextic operator becomes more and more relevant as the Higgs fluctuations become more and more classically unstable, thereby probing the new-physics scales. In essence, the presence of the additional higher-order operator rescues the parameter space excluded by stability constraints and leads to a GW signal that could not be produced within the SM effective potential. The three benchmark examples demonstrate that the SGWB signal possesses distinctive features at very high frequencies that provide us with useful information about the presence of non-renormalisable operators in the SM Higgs potential.

6 Conclusions

Vacuum stability is one of the most profound questions in fundamental physics, directly tied to the structure of the Higgs potential and the long-term fate of our Universe. One of the most significant outcomes of the Large Hadron Collider has been its ability to probe the stability of the electroweak vacuum by precisely measuring the Higgs boson and top quark masses, two key parameters that determine whether the vacuum is absolutely stable, metastable, or prone to decay over cosmological timescales. Intriguingly, current measurements place the SM vacuum near a critical boundary between stability and metastability, suggesting the possibility of new physics at higher energy scales. This delicate balance opens a compelling avenue for exploring BSM physics, as even slight modifications to the Higgs potential, such as new scalar fields, non-renormalisable interactions, or quantum gravity effects, could dramatically alter the fate of the vacuum.

The present work aims at probing the high-scale Higgs effective potential via GWs. The interplay of non-minimal gravitational couplings and a kination epoch results in a Hubble-induced phase transition that quickly reheats the Universe in a non-perturbative way while leaving a specific top-mass-dependent GW signature. We have shown that top

quark masses compatible with absolute stability generate a strong signal, while higher top quark masses enforce more stringent upper bounds on the inflationary scale, thus weakening the overall signal. A simultaneous detection of the inflationary background by low-frequency experiments and of the peak of the phase transition’s spectrum by ultra-high-frequency detectors can quantify the model parameters. In this sense, the scenario under consideration offers a way to investigate gravitationally the magnitude of the top quark mass. Notably, while the peak frequency of the spectrum is strongly correlated with the top quark mass, the reheating temperature is predominantly determined by the effective tachyonic mass. Different cosmological constraints can act complementarily in characterising the gravitational and Standard-Model couplings of the Higgs at high scales.

A key aspect of the analysis is the extensive use of parametric formulas, derived from hundreds of classical lattice simulations, which enable us to predict the general shape of the SGWB as a function of the top quark mass, being this quantity the largest source of uncertainty in the stability of the electroweak vacuum. It has to be noted that, unlike in other works on GWs from vacuum instability [68], our setup does not rely on the temporary instability of the Higgs vacuum to generate a GW signal. On the contrary, we have shown that a GW signal is unavoidable even in the case of absolute stability because of the combination of non-minimal curvature couplings and a stiff post-inflationary expansion phase.

We have also speculated about the possibility of BSM physics affecting the Higgs potential through non-renormalisable operators at scales below the cut-off dictated by the self-consistency of the theory. In this case, the positioning of the spectrum and its intrinsic characteristics can allow a direct link between the produced GW signal and the nature of such new interactions. This result can prompt some very interesting questions within the scenario of a non-minimally coupled Higgs field: Could specific patterns in the GW signal serve as a smoking gun for specific BSM extensions, such as Higgs portal models or new scalar fields coupled to the Higgs? Do these new interactions leave unique fingerprints in the Higgs potential, altering its phase structure in ways we can detect? How can we implement a consistent picture of quantum tunnelling in a stochastic system with a non-homogeneous and time-dependent fluctuating Higgs field? Can the interactions between the Higgs field and other thermal bath components leave detectable imprints on the GW spectrum? We plan to explore these questions in future publications.

Acknowledgments

We extend our gratitude to Dario Bettoni for engaging discussions that contributed to the preparation of this work. The numerical lattice simulations were carried out with the support of the Infraestrutura Nacional de Computação Distribuída (INCD) funded by the Fundação para a Ciência e a Tecnologia (FCT) and FEDER under the project 01/SAICT/2016 n^o 022153. G. L. acknowledges support from a fellowship provided by “la Caixa” Foundation (ID 100010434) with fellowship code LCF/BQ/DI21/11860024, as well as the support of FCT through the grant with Ref. 2024.05847.BD. G. L. acknowledges also the financial support from FCT to the Center for Astrophysics and Gravitation-CENTRA,

Instituto Superior Técnico, Universidade de Lisboa, through Project No. UIDB/00099/2020. J. R. is supported by a Ramón y Cajal contract of the Spanish Ministry of Science and Innovation with Ref. RYC2020-028870-I. This research was further supported by the project PID2022-139841NB-I00 of MICIU/AEI/10.13039/501100011033 and FEDER, UE.

A Summary of parametric formulas

In this Appendix, we present the full set of parametric formulas derived in [40, 67]. In order to be as general as possible, we keep the notation in those works, namely the dependence on λ and ν taken as tree-level parameters. At backreaction time z_{br} , the amplitude and the energy density are given by

$$\langle h_{\text{tac}}^2(\lambda, \nu) \rangle = 4\mathcal{H}_{\text{kin}}^2 \exp(\alpha_1 + \alpha_2 \nu + \alpha_3 \log \nu), \quad (\text{A.1})$$

$$\alpha_1 = -4.92 + 0.74 n, \quad \alpha_2 = -0.04 - 0.02 n, \quad \alpha_3 = 3.54 + 0.61 n, \quad (\text{A.2})$$

and

$$\rho_{\text{tac}}(\lambda, \nu) = 16 \mathcal{H}_{\text{kin}}^4 \exp(\beta_1 + \beta_2 \nu + \beta_3 \log \nu), \quad (\text{A.3})$$

$$\beta_1 = -7.03 - 0.56 n, \quad \beta_2 = -0.06 - 0.04 n, \quad \beta_3 = 7.15 + 1.10 n, \quad (\text{A.4})$$

with $\nu = \sqrt{3\xi/2}$ and $n = -\log_{10}(\lambda)$. The time at which the Higgs energy density achieves a radiation-like scaling is

$$z_{\text{rad}}(\lambda, \nu) = \gamma_1 + \gamma_2 \nu, \quad (\text{A.5})$$

$$\gamma_1 = 33.63 + 15.02 n - 0.22 n^2, \quad \gamma_2 = 7.91 - 0.01 n + 0.02 n^2, \quad (\text{A.6})$$

and the Higgs energy density at that timescale is

$$\rho_{\text{rad}}(\lambda, \nu) = 16\mathcal{H}_{\text{kin}}^4 \exp(\delta_1 + \delta_2 \nu + \delta_3 \log \nu), \quad (\text{A.7})$$

$$\delta_1 = -11.10 - 0.06 n, \quad \delta_2 = -0.04 - 0.03 n, \quad \delta_3 = 5.62 + 0.87 n. \quad (\text{A.8})$$

Note that \mathbb{Z}_2 -symmetric lattice simulations of real scalar fields give identical results (in terms of average amplitudes and energies) to those for $U(1)$ -symmetric complex fields in the unitary gauge, since there exists only one physical, real and positive-definite degree of freedom that follows the same averaged dynamics of a real scalar field in a \mathbb{Z}_2 -symmetric potential.

B Setting up classical lattice simulations

Our numerical analysis of the Higgs dynamics in its effective potential is carried out using the *CosmoLattice* code [49, 71] following the general procedure introduced in previous works [27, 40, 67]. The first step consists in implementing the full effective potential in a model file that includes a curvature-dependent effective mass, the three-loop RGI running of $\lambda(\mu)$ in (2.2) with an explicit dependence on the top quark and Higgs masses and the additional higher-order operator in (5.1). The lattice parameters are chosen to guarantee the stability of the solution and the covering of all relevant scales.

- The number of lattice points per dimension has been fixed to $N = 960$ with IR and UV momenta being defined by $\kappa_{\text{IR}} = 2\pi/L$, $\kappa_{\text{UV}} = \sqrt{3}N\kappa_{\text{IR}}/2$, where the lattice size is $L = N\delta x$ and $\delta x = 4\pi\nu/N$ is the dimension of a single lattice cell. From the discussion in [41], we set the smallest momentum in the tachyonic band with $\kappa_{\text{IR}} = \mathcal{H}_{\text{kin}}$, while the largest amplified momentum is set to be much smaller than the lattice's UV momentum, i.e. $\sqrt{4\nu^2 - 1}\mathcal{H}_{\text{kin}} \ll \kappa_{\text{UV}}$.
- The time-step is chosen according to the stability constraint $\delta t/\delta x \ll 1/\sqrt{d}$ [71], with $d = 3$ the number of spatial dimensions. The stiff background expansion is simply obtained by fixing the equation-of-state parameter to $w = 1$.
- A symplectic 4th order Velocity-Verlet method is used to evolve the scalar field. The initial conditions for our 3+1 classical lattice simulations are set as $h(0) = h'(0) = 0$, in agreement with the inflationary picture in [41]. Fluctuations over this homogeneous background are included as Gaussian random fields, as done customarily for systems with short classicalisation timescales [39]. The evolution is deterministic up to a randomised base seed that we choose to keep constant. Such a choice does not influence the evolution of the system, since it quickly loses memory of its initial state.
- The computation of the GW spectrum is obtained by solving the modified equation of motion for metric perturbations computed in [67] that take into account the presence of non-minimal interactions within the spectator field approximation.

References

- [1] F.L. Bezrukov and M. Shaposhnikov, *The Standard Model Higgs boson as the inflaton*, *Phys. Lett. B* **659** (2008) 703 [0710.3755].
- [2] F. Bauer and D.A. Demir, *Inflation with Non-Minimal Coupling: Metric versus Palatini Formulations*, *Phys. Lett. B* **665** (2008) 222 [0803.2664].
- [3] J. Garcia-Bellido, D.G. Figueroa and J. Rubio, *Preheating in the Standard Model with the Higgs-Inflaton coupled to gravity*, *Phys. Rev. D* **79** (2009) 063531 [0812.4624].
- [4] J.L.F. Barbon and J.R. Espinosa, *On the Naturalness of Higgs Inflation*, *Phys. Rev. D* **79** (2009) 081302 [0903.0355].
- [5] F. Bezrukov and M. Shaposhnikov, *Standard Model Higgs boson mass from inflation: Two loop analysis*, *JHEP* **07** (2009) 089 [0904.1537].
- [6] F. Bauer and D.A. Demir, *Higgs-Palatini Inflation and Unitarity*, *Phys. Lett. B* **698** (2011) 425 [1012.2900].
- [7] C.P. Burgess, H.M. Lee and M. Trott, *Comment on Higgs Inflation and Naturalness*, *JHEP* **07** (2010) 007 [1002.2730].
- [8] F. Bezrukov, A. Magnin, M. Shaposhnikov and S. Sibiryakov, *Higgs inflation: consistency and generalisations*, *JHEP* **01** (2011) 016 [1008.5157].
- [9] G.F. Giudice and H.M. Lee, *Unitarizing Higgs Inflation*, *Phys. Lett. B* **694** (2011) 294 [1010.1417].

- [10] F. Bezrukov and M. Shaposhnikov, *Higgs inflation at the critical point*, *Phys. Lett. B* **734** (2014) 249 [[1403.6078](#)].
- [11] Y. Hamada, H. Kawai, K.-y. Oda and S.C. Park, *Higgs inflation from Standard Model criticality*, *Phys. Rev. D* **91** (2015) 053008 [[1408.4864](#)].
- [12] D.P. George, S. Mooij and M. Postma, *Quantum corrections in Higgs inflation: the Standard Model case*, *JCAP* **04** (2016) 006 [[1508.04660](#)].
- [13] J. Repond and J. Rubio, *Combined Preheating on the lattice with applications to Higgs inflation*, *JCAP* **1607** (2016) 043 [[1604.08238](#)].
- [14] J. Fumagalli and M. Postma, *UV (in)sensitivity of Higgs inflation*, *JHEP* **05** (2016) 049 [[1602.07234](#)].
- [15] F. Bezrukov, M. Pauly and J. Rubio, *On the robustness of the primordial power spectrum in renormalized Higgs inflation*, *JCAP* **02** (2018) 040 [[1706.05007](#)].
- [16] J. Rubio and E.S. Tomberg, *Preheating in Palatini Higgs inflation*, *JCAP* **04** (2019) 021 [[1902.10148](#)].
- [17] M. Shaposhnikov, A. Shkerin and S. Zell, *Quantum Effects in Palatini Higgs Inflation*, *JCAP* **07** (2020) 064 [[2002.07105](#)].
- [18] F. Dux, A. Florio, J. Klarić, A. Shkerin and I. Timiryasov, *Preheating in Palatini Higgs inflation on the lattice*, *JCAP* **09** (2022) 015 [[2203.13286](#)].
- [19] A. Poisson, I. Timiryasov and S. Zell, *Critical points in Palatini Higgs inflation with small non-minimal coupling*, *JHEP* **03** (2024) 130 [[2306.03893](#)].
- [20] J. Rubio, *Higgs inflation*, *Front. Astron. Space Sci.* **5** (2019) 50 [[1807.02376](#)].
- [21] T. Markkanen, S. Nurmi and A. Rajantie, *Do metric fluctuations affect the Higgs dynamics during inflation?*, *JCAP* **12** (2017) 026 [[1707.00866](#)].
- [22] T. Markkanen, *Light scalars on cosmological backgrounds*, *JHEP* **01** (2018) 116 [[1711.07502](#)].
- [23] M. Herranen, T. Markkanen, S. Nurmi and A. Rajantie, *Spacetime curvature and the Higgs stability during inflation*, *Phys. Rev. Lett.* **113** (2014) 211102 [[1407.3141](#)].
- [24] M. Herranen, T. Markkanen, S. Nurmi and A. Rajantie, *Spacetime curvature and Higgs stability after inflation*, *Phys. Rev. Lett.* **115** (2015) 241301 [[1506.04065](#)].
- [25] D.G. Figueroa, J. Garcia-Bellido and F. Torrenti, *Decay of the standard model Higgs field after inflation*, *Phys. Rev.* **D92** (2015) 083511 [[1504.04600](#)].
- [26] T. Opferkuch, P. Schwaller and B.A. Stefanek, *Ricci Reheating*, *JCAP* **1907** (2019) 016 [[1905.06823](#)].
- [27] G. Laverda and J. Rubio, *The rise and fall of the Standard-Model Higgs: electroweak vacuum stability during inflation*, *JHEP* **05** (2024) 339 [[2402.06000](#)].
- [28] N.D. Birrell and P.C.W. Davies, *Quantum Fields in Curved Space*, Cambridge Monographs on Mathematical Physics, Cambridge Univ. Press, Cambridge, UK (1984), [10.1017/CBO9780511622632](#).
- [29] Y. Akrami, R. Kallosh, A. Linde and V. Vardanyan, *Dark energy, α -attractors, and large-scale structure surveys*, *JCAP* **1806** (2018) 041 [[1712.09693](#)].

- [30] K. Dimopoulos and C. Owen, *Quintessential Inflation with α -attractors*, *JCAP* **1706** (2017) 027 [[1703.00305](#)].
- [31] K. Dimopoulos, L. Donaldson Wood and C. Owen, *Instant preheating in quintessential inflation with α -attractors*, *Phys. Rev.* **D97** (2018) 063525 [[1712.01760](#)].
- [32] C. García-García, E.V. Linder, P. Ruíz-Lapuente and M. Zumalacárregui, *Dark energy from α -attractors: phenomenology and observational constraints*, *JCAP* **1808** (2018) 022 [[1803.00661](#)].
- [33] C. Wetterich, *Cosmology and the Fate of Dilatation Symmetry*, *Nucl. Phys.* **B302** (1988) 668 [[1711.03844](#)].
- [34] C. Wetterich, *The Cosmon model for an asymptotically vanishing time dependent cosmological 'constant'*, *Astron. Astrophys.* **301** (1995) 321 [[hep-th/9408025](#)].
- [35] J. Rubio and C. Wetterich, *Emergent scale symmetry: Connecting inflation and dark energy*, *Phys. Rev.* **D96** (2017) 063509 [[1705.00552](#)].
- [36] Y. Gouttenoire, G. Servant and P. Simakachorn, *Kination cosmology from scalar fields and gravitational-wave signatures*, [2111.01150](#).
- [37] P.J.E. Peebles and A. Vilenkin, *Quintessential inflation*, *Phys. Rev.* **D59** (1999) 063505 [[astro-ph/9810509](#)].
- [38] B. Spokoiny, *Deflationary universe scenario*, *Phys. Lett.* **B315** (1993) 40 [[gr-qc/9306008](#)].
- [39] D. Bettoni, A. Lopez-Eiguren and J. Rubio, *Hubble-induced phase transitions on the lattice with applications to Ricci reheating*, *JCAP* **01** (2022) 002 [[2107.09671](#)].
- [40] G. Laverda and J. Rubio, *Ricci reheating reloaded*, *JCAP* **03** (2024) 033 [[2307.03774](#)].
- [41] D. Bettoni and J. Rubio, *Hubble-induced phase transitions: Walls are not forever*, *JCAP* **01** (2020) 002 [[1911.03484](#)].
- [42] D. Bettoni and J. Rubio, *Quintessential Affleck-Dine baryogenesis with non-minimal couplings*, *Phys. Lett.* **B784** (2018) 122 [[1805.02669](#)].
- [43] D. Bettoni, G. Doménech and J. Rubio, *Gravitational waves from global cosmic strings in quintessential inflation*, *JCAP* **1902** (2019) 034 [[1810.11117](#)].
- [44] A. Mantziris and O. Bertolami, *Gravitational waves from a curvature-induced phase transition of a Higgs-portal dark matter sector*, *JCAP* **10** (2024) 104 [[2407.18845](#)].
- [45] M. Kierkla, G. Laverda, M. Lewicki, A. Mantziris, M. Piani, J. Rubio et al., *From Hubble to Bubble*, *JHEP* **11** (2023) 077 [[2309.08530](#)].
- [46] K. Kohri and H. Matsui, *Higgs vacuum metastability in primordial inflation, preheating, and reheating*, *Phys. Rev. D* **94** (2016) 103509 [[1602.02100](#)].
- [47] D.G. Figueroa and C.T. Byrnes, *The Standard Model Higgs as the origin of the hot Big Bang*, *Phys. Lett.* **B767** (2017) 272 [[1604.03905](#)].
- [48] D.G. Figueroa, A. Rajantie and F. Torrenti, *Higgs field-curvature coupling and postinflationary vacuum instability*, *Phys. Rev. D* **98** (2018) 023532 [[1709.00398](#)].
- [49] D.G. Figueroa and F. Torrenti, *Parametric resonance in the early Universe—a fitting analysis*, *JCAP* **1702** (2017) 001 [[1609.05197](#)].
- [50] A. Mantziris, T. Markkanen and A. Rajantie, *Vacuum decay constraints on the Higgs curvature coupling from inflation*, *JCAP* **03** (2021) 077 [[2011.03763](#)].

- [51] A. Mantziris, *Cosmological implications of EW vacuum instability: constraints on the Higgs-curvature coupling from inflation*, *PoS EPS-HEP2021* (2022) 127 [2111.02464].
- [52] A. Mantziris, *On the cosmological implications of the electroweak vacuum instability: constraining the non-minimal coupling with inflation*, *J. Phys. Conf. Ser.* **2156** (2021) 012239 [2111.02497].
- [53] A. Mantziris, *Ending inflation with a bang: Higgs vacuum decay in R^2 gravity*, *PoS ICHEP2022* (2022) 114 [2211.09244].
- [54] A. Mantziris, T. Markkanen and A. Rajantie, *The effective Higgs potential and vacuum decay in Starobinsky inflation*, *JCAP* **10** (2022) 073 [2207.00696].
- [55] A. Mantziris, *Higgs vacuum metastability in $R + R^2$ gravity*, in *40th Conference on Recent Developments in High Energy Physics and Cosmology*, 8, 2023 [2308.00779].
- [56] M. Postma and J. van de Vis, *Electroweak stability and non-minimal coupling*, *JCAP* **1705** (2017) 004 [1702.07636].
- [57] Y. Ema, M. Karciauskas, O. Lebedev and M. Zatta, *Early Universe Higgs dynamics in the presence of the Higgs-inflaton and non-minimal Higgs-gravity couplings*, *JCAP* **06** (2017) 054 [1703.04681].
- [58] K. Enqvist, M. Karciauskas, O. Lebedev, S. Rusak and M. Zatta, *Postinflationary vacuum instability and Higgs-inflaton couplings*, *JCAP* **11** (2016) 025 [1608.08848].
- [59] Y. Ema, K. Mukaida and K. Nakayama, *Fate of Electroweak Vacuum during Preheating*, *JCAP* **10** (2016) 043 [1602.00483].
- [60] P.F. de Salas, M. Lattanzi, G. Mangano, G. Miele, S. Pastor and O. Pisanti, *Bounds on very low reheating scenarios after Planck*, *Phys. Rev. D* **92** (2015) 123534 [1511.00672].
- [61] T. Hasegawa, N. Hiroshima, K. Kohri, R.S.L. Hansen, T. Tram and S. Hannestad, *MeV-scale reheating temperature and thermalization of oscillating neutrinos by radiative and hadronic decays of massive particles*, *JCAP* **12** (2019) 012 [1908.10189].
- [62] Y. Tang, *Vacuum Stability in the Standard Model*, *Mod. Phys. Lett. A* **28** (2013) 1330002 [1301.5812].
- [63] J.R. Espinosa, G.F. Giudice, E. Morgante, A. Riotto, L. Senatore, A. Strumia et al., *The cosmological Higgstory of the vacuum instability*, *JHEP* **09** (2015) 174 [1505.04825].
- [64] G. Hiller, T. Höhne, D.F. Litim and T. Steudtner, *Vacuum stability in the Standard Model and beyond*, *Phys. Rev. D* **110** (2024) 115017 [2401.08811].
- [65] CMS collaboration, *Measurement of $t\bar{t}$ normalised multi-differential cross sections in pp collisions at $\sqrt{s} = 13$ TeV, and simultaneous determination of the strong coupling strength, top quark pole mass, and parton distribution functions*, *Eur. Phys. J. C* **80** (2020) 658 [1904.05237].
- [66] CMS collaboration, *Measurement of the top quark mass using a profile likelihood approach with the lepton + jets final states in proton-proton collisions at $\sqrt{s} = 13$ TeV*, *Eur. Phys. J. C* **83** (2023) 963 [2302.01967].
- [67] D. Bettoni, G. Laverda, A.L. Eiguren and J. Rubio, *Hubble-Induced Phase Transitions: Gravitational-Wave Imprint of Ricci Reheating from Lattice Simulations*, **2409.15450**.
- [68] J.R. Espinosa, D. Racco and A. Riotto, *A Cosmological Signature of the SM Higgs Instability: Gravitational Waves*, *JCAP* **09** (2018) 012 [1804.07732].

- [69] T. Markkanen, S. Nurmi, A. Rajantie and S. Stopyra, *The 1-loop effective potential for the Standard Model in curved spacetime*, *JHEP* **06** (2018) 040 [[1804.02020](#)].
- [70] PARTICLE DATA GROUP collaboration, *Review of particle physics*, *Phys. Rev. D* **110** (2024) 030001.
- [71] D.G. Figueroa, A. Florio, F. Torrenti and W. Valkenburg, *CosmoLattice: A modern code for lattice simulations of scalar and gauge field dynamics in an expanding universe*, *Comput. Phys. Commun.* **283** (2023) 108586 [[2102.01031](#)].
- [72] V. Mukhanov and S. Winitzki, *Introduction to quantum effects in gravity*, Cambridge University Press (6, 2007).
- [73] D.G. Figueroa, T. Opferkuch and B.A. Stefanek, *Ricci Reheating on the Lattice*, [2404.17654](#).
- [74] P.B. Greene, L. Kofman, A.D. Linde and A.A. Starobinsky, *Structure of resonance in preheating after inflation*, *Phys. Rev.* **D56** (1997) 6175 [[hep-ph/9705347](#)].
- [75] K. Enqvist, S. Nurmi, S. Rusak and D. Weir, *Lattice Calculation of the Decay of Primordial Higgs Condensate*, *JCAP* **1602** (2016) 057 [[1506.06895](#)].
- [76] D. Bodeker and K. Rummukainen, *Non-abelian plasma instabilities for strong anisotropy*, *JHEP* **07** (2007) 022 [[0705.0180](#)].
- [77] F. Bezrukov, J. Rubio and M. Shaposhnikov, *Living beyond the edge: Higgs inflation and vacuum metastability*, *Phys. Rev. D* **92** (2015) 083512 [[1412.3811](#)].
- [78] J. Rubio, *Higgs inflation and vacuum stability*, *J. Phys. Conf. Ser.* **631** (2015) 012032 [[1502.07952](#)].
- [79] R. Micha and I.I. Tkachev, *Turbulent thermalization*, *Phys. Rev.* **D70** (2004) 043538 [[hep-ph/0403101](#)].
- [80] J. Garcia-Bellido, D.G. Figueroa and J. Rubio, *Preheating in the Standard Model with the Higgs-Inflaton coupled to gravity*, *Phys. Rev.* **D79** (2009) 063531 [[0812.4624](#)].
- [81] M. Lewicki and V. Vaskonen, *Gravitational waves from colliding vacuum bubbles in gauge theories*, *Eur. Phys. J. C* **81** (2021) 437 [[2012.07826](#)].
- [82] M. Lewicki and V. Vaskonen, *Gravitational waves from bubble collisions and fluid motion in strongly supercooled phase transitions*, *Eur. Phys. J. C* **83** (2023) 109 [[2208.11697](#)].
- [83] C. Caprini, R. Durrer, T. Konstandin and G. Servant, *General Properties of the Gravitational Wave Spectrum from Phase Transitions*, *Phys. Rev. D* **79** (2009) 083519 [[0901.1661](#)].
- [84] R.-G. Cai, S. Pi and M. Sasaki, *Universal infrared scaling of gravitational wave background spectra*, *Phys. Rev. D* **102** (2020) 083528 [[1909.13728](#)].
- [85] R. Allahverdi, M.A. Amin, A. Berlin, N. Bernal, C.T. Byrnes, M.S. Delos et al., *The first three seconds: a review of possible expansion histories of the early universe*, *The Open Journal of Astrophysics* **4** (2021) .
- [86] PLANCK collaboration, *Planck 2018 results. X. Constraints on inflation*, *Astron. Astrophys.* **641** (2020) A10 [[1807.06211](#)].
- [87] P. Amaro-Seoane, H. Audley, S. Babak, J. Baker, E. Barausse, P. Bender et al., *Laser interferometer space antenna*, 2017.

- [88] T. Robson, N.J. Cornish and C. Liu, *The construction and use of LISA sensitivity curves*, *Class. Quant. Grav.* **36** (2019) 105011 [[1803.01944](#)].
- [89] J. Crowder and N.J. Cornish, *Beyond LISA: Exploring future gravitational wave missions*, *Phys. Rev. D* **72** (2005) 083005 [[gr-qc/0506015](#)].
- [90] V. Corbin and N.J. Cornish, *Detecting the cosmic gravitational wave background with the big bang observer*, *Class. Quant. Grav.* **23** (2006) 2435 [[gr-qc/0512039](#)].
- [91] N. Seto, S. Kawamura and T. Nakamura, *Possibility of direct measurement of the acceleration of the universe using 0.1-Hz band laser interferometer gravitational wave antenna in space*, *Phys. Rev. Lett.* **87** (2001) 221103 [[astro-ph/0108011](#)].
- [92] K. Yagi and N. Seto, *Detector configuration of DECIGO/BBO and identification of cosmological neutron-star binaries*, *Phys. Rev. D* **83** (2011) 044011 [[1101.3940](#)].
- [93] S. Kawamura et al., *Current status of space gravitational wave antenna DECIGO and B-DECIGO*, *PTEP* **2021** (2021) 05A105 [[2006.13545](#)].
- [94] M. Punturo et al., *The Einstein Telescope: A third-generation gravitational wave observatory*, *Class. Quant. Grav.* **27** (2010) 194002.
- [95] M. Branchesi et al., *Science with the Einstein Telescope: a comparison of different designs*, *JCAP* **07** (2023) 068 [[2303.15923](#)].
- [96] LIGO SCIENTIFIC collaboration, *Exploring the Sensitivity of Next Generation Gravitational Wave Detectors*, *Class. Quant. Grav.* **34** (2017) 044001 [[1607.08697](#)].
- [97] D. Reitze et al., *Cosmic Explorer: The U.S. Contribution to Gravitational-Wave Astronomy beyond LIGO*, *Bull. Am. Astron. Soc.* **51** (2019) 035 [[1907.04833](#)].
- [98] N. Herman, L. Lehoucq and A. Fúza, *Electromagnetic antennas for the resonant detection of the stochastic gravitational wave background*, *Phys. Rev. D* **108** (2023) 124009 [[2203.15668](#)].
- [99] C. Gatti, L. Visinelli and M. Zantedeschi, *Cavity detection of gravitational waves: Where do we stand?*, *Phys. Rev. D* **110** (2024) 023018 [[2403.18610](#)].
- [100] N. Aggarwal et al., *Challenges and opportunities of gravitational-wave searches at MHz to GHz frequencies*, *Living Rev. Rel.* **24** (2021) 4 [[2011.12414](#)].
- [101] R. Allahverdi et al., *The First Three Seconds: a Review of Possible Expansion Histories of the Early Universe*, [2006.16182](#).
- [102] T. Steingasser, M. König and D.I. Kaiser, *Finite-temperature instantons from first principles*, *Phys. Rev. D* **110** (2024) L111902 [[2310.19865](#)].
- [103] T. Steingasser and D.I. Kaiser, *Quantum tunneling from excited states: Recovering imaginary-time instantons from a real-time analysis*, [2402.00099](#).
- [104] B. Garbrecht and N. Wagner, *False vacuum decay of excited states in finite-time instanton calculus*, [2412.20431](#).
- [105] C.P. Burgess, H.M. Lee and M. Trott, *Power-counting and the Validity of the Classical Approximation During Inflation*, *JHEP* **09** (2009) 103 [[0902.4465](#)].
- [106] M.P. Hertzberg, *On Inflation with Non-minimal Coupling*, *JHEP* **11** (2010) 023 [[1002.2995](#)].

- [107] F. Bezrukov, G.K. Karananas, J. Rubio and M. Shaposhnikov, *Higgs-Dilaton Cosmology: an effective field theory approach*, *Phys. Rev. D* **87** (2013) 096001 [[1212.4148](#)].
- [108] J. Ren, Z.-Z. Xianyu and H.-J. He, *Higgs Gravitational Interaction, Weak Boson Scattering, and Higgs Inflation in Jordan and Einstein Frames*, *JCAP* **06** (2014) 032 [[1404.4627](#)].
- [109] J. Fumagalli, S. Mooij and M. Postma, *Unitarity and predictiveness in new Higgs inflation*, *JHEP* **03** (2018) 038 [[1711.08761](#)].
- [110] I. Antoniadis, A. Guillen and K. Tamvakis, *Ultraviolet behaviour of Higgs inflation models*, *JHEP* **08** (2021) 018 [[2106.09390](#)].
- [111] Y. Mikura and Y. Tada, *On UV-completion of Palatini-Higgs inflation*, *JCAP* **05** (2022) 035 [[2110.03925](#)].
- [112] A. Ito, W. Khater and S. Rasanen, *Tree-level unitarity in Higgs inflation in the metric and the Palatini formulation*, *JHEP* **06** (2022) 164 [[2111.05621](#)].
- [113] A. Escrivà and C. Germani, *Beyond dimensional analysis: Higgs and new Higgs inflations do not violate unitarity*, *Phys. Rev. D* **95** (2017) 123526 [[1612.06253](#)].
- [114] G.K. Karananas, M. Shaposhnikov and S. Zell, *Field redefinitions, perturbative unitarity and Higgs inflation*, *JHEP* **06** (2022) 132 [[2203.09534](#)].
- [115] U. Aydemir, M.M. Anber and J.F. Donoghue, *Self-healing of unitarity in effective field theories and the onset of new physics*, *Phys. Rev. D* **86** (2012) 014025 [[1203.5153](#)].
- [116] X. Calmet and R. Casadio, *Self-healing of unitarity in Higgs inflation*, *Phys. Lett. B* **734** (2014) 17 [[1310.7410](#)].
- [117] I.D. Saltas, *Higgs inflation and quantum gravity: An exact renormalisation group approach*, *JCAP* **02** (2016) 048 [[1512.06134](#)].
- [118] A. Eichhorn, H. Gies, J. Jaeckel, T. Plehn, M.M. Scherer and R. Sondenheimer, *The Higgs Mass and the Scale of New Physics*, *JHEP* **04** (2015) 022 [[1501.02812](#)].
- [119] V. Branchina and E. Messina, *Stability, Higgs Boson Mass and New Physics*, *Phys. Rev. Lett.* **111** (2013) 241801 [[1307.5193](#)].
- [120] D.G. Figueroa, A. Florio, F. Torrenti and W. Valkenburg, *The art of simulating the early Universe – Part I*, *JCAP* **04** (2021) 035 [[2006.15122](#)].